Atmospheric
Chemistry
and Physics
Discussions

Response of atmospheric composition to COVID-19 lockdown measures during Spring in the Paris region (France)

Jean-Eudes Petit[1], Jean-Charles Dupont[2], Olivier Favez[3], Valérie Gros[1], Yunjiang Zhang[1,3], Jean Sciare[1*], Leila Simon[1,3], François Truong[1], Nicolas Bonnaire[1], Tanguy Amodeo[3], Robert Vautard[1], Martial Haeffelin[4]

5   [1]Laboratoire des Sciences du Climat et de l'Environnement, CEA/Orme des Merisiers, Gif-sur-Yvette, France
[2]Institut Pierre Simon Laplace, Ecole Polytechnique, UVSQ, Université Paris-Saclay, Palaiseau, France
[3]Institut National de l'Environnement Industriel et des Risques, Parc Technologique ALATA, Verneuil en Halatte, France
[4]Institut Pierre Simon Laplace, Ecole Polytechnique, CNRS, Université Paris-Saclay, Palaiseau, France
[*] Now at Cyprus Institute, Nicosia, Cyprus

10 *Correspondence to*: Jean-Eudes Petit (jean-eudes.petit@lsce.ipsl.fr)

Abstract. Since early 2020, the COVID-19 pandemic has led to lockdowns at national scales. These lockdowns resulted in large cuts of atmospheric pollutant emissions, notably related to the vehicular traffic source where daily commuting of light-duty vehicles was almost completely stopped in numerous urban areas worldwide, especially during Spring 2020. As a result, air quality changed in manners that are still currently under investigation. Long-term in-situ monitoring of atmospheric composition provides, to this perspective, essential information. However, a robust quantitative assessment of the impact of lockdown measures on ambient concentrations is hindered by weather variability. Basic comparisons with previous years may thus be flawed, especially regarding secondary pollutants, whose concentrations strongly depends on meteorological conditions. In order to circumvent this difficulty, an innovative methodology has been developed. The Analog Application for Air Quality (A³Q) method is based on the comparison of each day of lockdown to a group of analog days having similar meteorological conditions. The A³Q method has been successfully evaluated and applied to a comprehensive in-situ dataset of primary and secondary pollutants obtained at the SIRTA observatory, a suburban background site of the Paris megacity (France). The overall slight decrease of PM_1 concentrations (-14%) compared to business-as-usual conditions conceals contrasting behaviours. Primary traffic tracers (NO_x and traffic-related carbonaceous aerosols) dropped by 42-66% during the lockdown period. Further, the A³Q method enabled us to characterize of changes triggered by NO_x decreases. Particulate nitrate and secondary organic aerosols (SOA), two of the main springtime aerosol components in North-Western Europe, decreased by -45% and -25%, respectively. A NO_x-relationship emphasizes the interest of NO_x mitigation policies at the regional (i.e. city) scale, although long-range pollution advection sporadically overcompensated regional decreases. Variations of the oxidation state of SOA suggests discrepancies in SOA formation processes. At the same time, the expected ozone increase (+20%) underlines the negative feedback of NO titration. These results provide a quasi-comprehensive observation-based insight on mitigation policies regarding air quality in future low-carbon urban areas.

1. Introduction

35   With the worldwide spreading of the SARS-COV-2 coronavirus, the COVID-19 outbreak has been responsible of millions of premature deaths. In order to slow down contagion rates, social interactions have progressively been limited until the establishment of strict lockdowns at national scales (Anderson et al., 2020) enforced

Atmospheric
Chemistry
and Physics
Discussions
Open Access

during several weeks, especially during Spring 2020 in Europe. The corresponding stay-at-home orders resulted in a sudden halt of economic activities, and, as a consequence, in an unprecedented drop of emission

40   of pollution sources. To this perspective, and despite tragic death records, these lockdowns are unique opportunities to characterize an extreme end of mitigation policy scenarios, and future low-carbon megacities from direct observations.

Scientific initiatives are thriving across the globe in order to assess the impact of lockdowns on air quality. They report, for most, a sharp decrease of nitrogen oxides (NO_x) concentrations, as well as an increase of

45   troposheric ozone (e.g. China: Le et al. (2020); India: Mahato et al. (2020); USA: Liu et al. (2020a); Europe: Sicard et al. (2020); Grange et al. (2020); South-America: Siciliano et al. (2020)) as a response to stay-at-home orders. However, despite this luxuriance of literature, the assessment of air quality implications of large cuts in urban pollutant emissions is strongly hampered by meteorological variability, which is one of the main drivers of air pollution temporality. Without climatologically representative values, comparisons of

50   concentrations observed during and outside the lockdown periods shall thus free themselves from differences in weather. The robustness of this assessment depends on the way meteorology is handled and on what "reference period" is chosen to compare with the "lockdown period". Recently, advances on machine-learning (ML) approaches have enabled to unknot the contributions of meteorological conditions into weather-normalized timeseries (e.g. Stirnberg et al., 2021). ML has successfully been applied mainly on

55   NO_x and O_3 in various urban areas (Petetin et al., 2020; Grange et al., 2020), but little information are being gathered on PM and its chemical constituents. Air quality shall not be restrained to NO_x, O_3 and PM_x only, and limited number of studies so far have treated air quality as a whole, notably by taking PM chemistry into account (Kroll et al., 2020). Indeed, PM is composed of several different fractions, from organic to inorganic, and from primary to secondary pollutants, with diverse sources and transformation processes. Any

60   concentration change of PM may derive from various compensatory feedbacks which are not characterized, limiting therefore our understanding of the impacts of lockdown on air quality. Moreover, Springtime in North-Western Europe is usually associated with high PM pollution episodes dominated by secondary material (mainly ammonium nitrate and sulfate, and secondary organic aerosols) as shown in Petit et al. (2015), Beekmann et al. (2015), Petit et al. (2017a) for instance. To this perspective, the complex chemistry of PM must

65   be taken into account, emphasizing the need of in-situ aerosol chemical characterization data.

The present study aims at reconciling a robust and innovative methodology with a quasi-comprehensive in-situ dataset, acquired within the Paris region (France). The 12-million inhabitants of the region, representing around 20% of the total French population, were placed under lockdown from March 17th, 2020 to May 10th, 2020, further designated as LP2020.

70

2. In-situ characterization of the atmospheric composition

2.1. Instrumentation

In-situ measurement datasets used in this study have been primarily obtained at the SIRTA atmospheric observatory (2.15°E, 48.71°N; Haeffelin et al., 2005), a facility which contributes to the EU-research

75   infrastructure ACTRIS (https://www.actris.eu), following its Quality assurance / Quality control guidelines.
The chemical composition of major submicron non-refractory species has been monitored since the end of
2011 using an Aerosol Chemical Speciation Monitor (ACSM, Ng et al., 2011), constituting the longest ACSM
dataset worldwide. Measurement principles of the ACSM are extensively described elsewhere
(Budisulistiorini et al., 2014; Zhang et al., 2019; Poulain et al., 2020). Here, 30-min concentrations of submicron

80   Organic Aerosols (OA), Nitrate (NO_3), Sulfate (SO_4), Ammonium (NH_4) and Chloride (Cl) were corrected from
collection efficiency (Middlebrook et al., 2012) (CE). The ACSM at SIRTA was regularly calibrated using 300-
nm ammonium nitrate and ammonium sulfate particles to derive Ionization Efficiencies (IE), and successfully
participated in ACTRIS intercomparaison exercises (Crenn et al., 2015; Freney et al., 2019).

The black carbon dataset consists in Aethalometer measurements (Drinovec et al., 2015). It is composed of

85   subsequent and harmonized datasets obtained from AE31 (01/2011-03/2013) and AE33 , 03/2013-06/2020)
devices and applying a common validation procedure (Petit et al., 2017b). Briefly, for each elementary
measurement data point (5-min and 1-min time-base for AE31 and AE33, respectively), BC_λ concentrations
were set as invalid when below -LoD (Limit of Detection, 100 ng/m^3); for $BC_{950nm} \geq 200$ ng/m^3, the spectral
dependence was calculated from the linear regression of $\ln(\lambda)$ versus $\ln(B_{atn})$. Measurements were considered

90   valid for a r^2 (of this linear regression) higher than 0.9 and Aerosol Angström Exponent (AAE) comprised
between 0.8 and 3.

Daily concentrations of nitrogen monoxide (NO) and nitrogen dioxide (NO_2) were retrieved from 1-min
measurements performed with a T200UP Teledyne instrument, equipped with a blue light photolytic
converter and a Nafion dryer. The instrument has been regularly calibrated with a reference standard from

95   National Physics Laboratory (Teddington, UK) and NO and NO_2 concentrations have been corrected from
ozone interference. The NO_x analyzer has participated to the 2 ACTRIS intercomparaison excercises
organized at Hohenpeissenberg in 2012 and 2016 and has shown a good comparability with other instruments.
Other NO_x observations throughout the Paris region between 2012 and 2020 were retrieved from the regional
air quality monitoring structure (Airparif, https://www.airparif.asso.fr). To this respect, urban NO_x

100   concentrations refer here to the average of all urban background stations measuring NO_x.

As the ozone instrument from SIRTA experienced a major breakdown in 2020, daily ozone (O_3) concentrations
were obtained between 2012 and 2020 from a peri-urban station in Les Ulis (2.165°E, 48.68°N), operated by
Airparif. This station is located around 10 km away from SIRTA and O_3 from Les Ulis has shown a good
comparability with O_3 from SIRTA during the period of common measurements.

105   Meteorological variables at SIRTA (wind speed and direction, temperature, relative humidity and pressure)
were provided from the ReObs database (Chiriaco et al., 2018).

2.2. Source apportionment of carbonaceous aerosols

A source apportionment study of OA was carried out by Positive Matrix Factorisation (PMF, Paatero and

110   Tapper, 1994) from January to May 2020. The analysis has been carried out seasonally (January-February and
March-April-May) in order to prevent from the seasonality of the profiles of secondary factors (Canonaco et
al., 2015). Profiles of Hydrocarbon-like Organic Aerosols (HOA), Biomass Burning Organic Aerosols (BBOA)

were constrained with a random a-value approach (Canonaco et al., 2013), a third factor being left unconstrained (Oxygenated Organic Aerosol, OOA). The criteria approach of SoFi Pro (Canonaco et al., 2020)

115 was then used to select satisfactory solutions over 100 runs, from the R-Pearson correlation of HOA vs BC_{ff}, HOA vs NO_x and BBOA vs BC_{wb}. Results obtained here enrich the existing timeseries (Zhang et al., 2019) from June 2011 to March 2018; together they form one of the longest ACSM PMF timeseries published to date. MO-OOA and LO-OOA were summed as OOA.

The oxidation properties of secondary organic aerosols were characterized by removing the contribution of

120 primary factors to the OA matrix, as follows:

$$f_i^{SOA} = \frac{m/z_i - (f_i^{HOA} \cdot [HOA] + f_i^{BBOA} \cdot [BBOA])}{[OA] - ([HOA] + [BBOA])}$$

From there, $O:C_{SOA}$, $H:C_{SOA}$ and OSc_{SOA} were calculated from the equations provided in (Aiken et al., 2008; Kroll et al., 2011; Canagaratna et al., 2014). These equations provide only qualitative information for ACSM data, but are sufficient to characterize a change, since they are uniformly applied throughout the dataset.

125

Fossil-fuel (BC_{ff}) and Biomass burning (BC_{wb}) fractions were estimated from aethalometer measurements (Sandradewi et al., 2008). Since the choice of α_{ff} and α_{wb} is critical and given the size of our dataset, their determination was based on the statistical hourly distribution of the AAE (Fig. S1). The value of 1.85 was chosen for α_{wb}, corresponding to a maximum frequency during the night. This value is close to the values used

130 previously at SIRTA (Zhang et al., 2019), and from the recommended value of 1.72 (Zotter et al., 2016). PM_{ff} and PM_{wb} were estimated from BC_{ff} and BC_{wb} concentrations, respectively, following the conversion factors of 2 and 10.3 found for SIRTA during the same season (Petit et al., 2014).

The full timeseries between 2012 and 2020 is presented in Figure S2.

135

2.3. Backtrajectory calculation

120-h backtrajectories ending at SIRTA (49.15°E, 2.19°N) at 500m a.g.l. were calculated every 6h from 2012 to 2020 with the PC-based version of HYSPLIT (Stein et al., 2015) using 1°x1° Global Data Assimilation System

140 (GDAS) files. Calculations were controlled by ZeFir (Petit et al., 2017a).

3. Methodology to estimate the impact of lockdown measures : an attempt to compare apples to apples

3.1. Choice of the comparison reference period

The assessment of lockdown impact on air quality lies on the use of a reference period, which is assumed to

145 be representative of business-as-usual conditions during LP2020, following:

$$\%change = 100 \cdot \frac{LP_{2020} - ref}{ref}$$

However, it can lead to some variability in the results, depending on the chosen reference period, representing therefore a critical issue. The major danger would be to apply methodologies unquestioningly,

150 without verifying the strong inherent hypothesis that data are comparable. For instance, one could consider the weeks preceding the lockdown period as a satisfactory reference (e.g., Toscano and Murena, 2020; Dantas et al., 2020; Otmani et al., 2020). In the case of SIRTA, we tried to compare the pollutant concentrations averaged over the lockdown period (LP 2020) to the ones calculated for the 20 previous days (pLP 2020 : 25/02/2020 - 16/03/2020). As shown in Figure 1, applying such a method led to the determination of

155 significant concentration increases for all pollutants during the lockdown period (e.g., + 83% in NO_x, +439% in PM_1), which seems to contradict the observed drop of traffic.
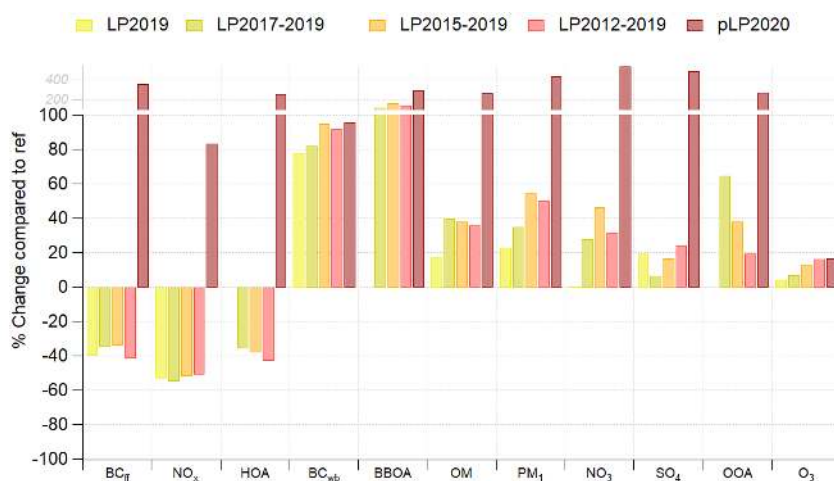
Figure 1 : Relative concentration change (%) of each specie used in this study following different reference
160 **periods.**

Alternatively, we tried to use the weeks corresponding to LP for previous years (e.g. 2017-2019, LP2017-2019) as the reference. Obtained results seemed to reveal a substantial decrease for the concentrations of pollutants related to traffic emissions (i.e., BC_{ff}, HOA and NO_x), but clear increases of all other investigated

165 pollutants, especially secondaries (Fig. 1). Similar results were obtained when narrowing (e.g., looking only at LP_{2019}, Mesas-Carrascosa et al., 2020) or broadening (e.g., $LP_{2012-2019}$ or $LP_{2015-2019}$, Adams, 2020; Sun et al., 2020) the reference period.

Applying such methodologies blindly encompasses interannual variability, and do not take potential long-term trends into account. Moreover, they inherently assume comparable meteorology. Figure 2a presents

170 the trajectory density during LP2020, showing a strong prevalence of continental air masses. When comparing the air mass origin of LP2020 and other reference periods (pLP2020, LP2019, LP2017-2019, LP2015-2019, LP2012-2019, Figure S3), it appears that the continental sector is under-represented, while the oceanic sector is over-represented (Fig. 2b). The unrealistic features of pLP2020 can then be explained by a drastic change of Western Europe meteorological conditions (from low-pressure to high-pressure system)

175 concomitantly with the application of lockdown policy measures in France, preventing for using such a

methodology in the present study. For the other reference periods, it may also explain why these methodologies are associated to an increase of eg NO_3, SO_4 and OOA, due to an underestimation of business-as-usual concentrations for LP2020 meteorological conditions. For this matter, and in order to avoid erroneous, contradictory and/or counterintuitive results, it appears critical to take synoptic circulation and air mass origin into account.
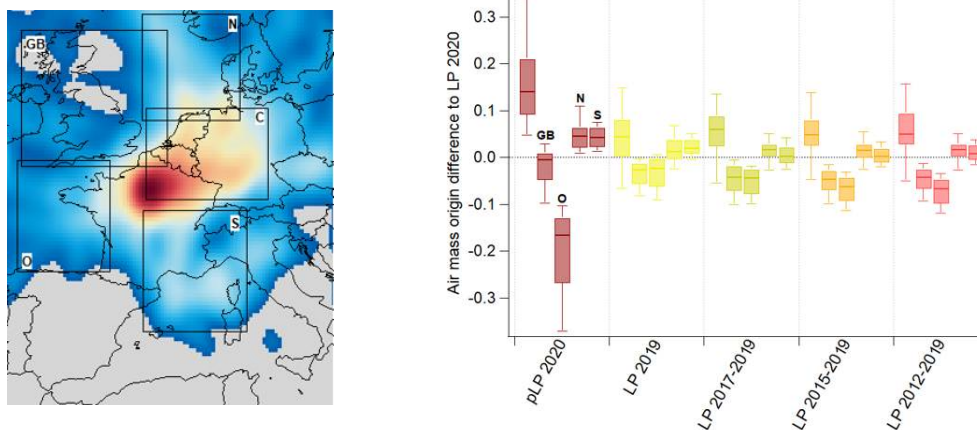

Figure 2: a) Air mass origin during LP2020, represented as trajectory density. b) Difference of air mass origin between LP2020 and the different reference periods (trajectory densities have been normalized to unity), divided into 5 main sectors (Continental, Great Britain, Oceanic, North, and South) delimited in a).

Additionally, April 2020 in France was exceptionally warmer (+4.5°C), drier (-43% of precipitation in the Paris region) and more sunny (+60%) than usual (1981-2010 climatological reference values). To this perspective, local meteorology needs to be taken into account as much as possible, since this climatological extreme may have favoured photochemical processes.

To overcome all these issues and account for the strong synergy between PM chemical composition, emission sources and meteorology, we developed the Analog Application for Air Quality (A^3Q) method, which is described below.

3.2. The "Analog Application for Air Quality" (A^3Q) approach

3.2.1. Description

Analogs of atmospheric circulation (Yiou et al., 2013; Lorenz, 1969; Van Den Dool, 1994; Zorita and Storch, 1999; Cattiaux et al., 2012) have been widely used for different climatological purposes, notably for atmospheric reconstructions and in the characterization of the role of synoptic circulation in extreme meteorological events (Yiou et al., 2013; Vautard et al., 2018). Circulation analogs are generally computed from daily pressure spatial distributions. Here, we built the analogy based on three successive layers:

Synoptic. Circulation analogs are computed similarly to previous studies. We used daily sea-level pressure (SLP) data, to better characterize near-surface atmospheric circulation as our study covers near-surface pollutants. The SLP data is extracted from NCEP/NCAR reanalysis data (Kalnay et al., 1996) along the

205 historical period that covers 2012 to 2019. The SLP fields considered here have a horizontal resolution of 2.5 x 2.5° and cover a spatial domain ranging -20°W to +15°E in longitude and +40°N to +60°N in latitude. This region is chosen because it includes atmospheric pressure patterns that influence near-surface wind (Raynaud et al., 2017) in our area of study. The study period covers 92 days from March 1st until May 31st 2020, while the historical period covers the same months in 2012-2019. Fifty best circulation analogs (minimum

210 spatial correlation of 0.5) are sought for each day of the study period, using the spatial correlation as a way to measure similarity between SLP fields. The calendar distance between the day in the study period and days in the historic period is maximum 30 days. Out of 50 potential days with analog atmospheric circulation, only those with a spatial correlation higher than 0.6 (representing 97.8% of all analog days, 23.2 analogs/day on average) were kept.

215 *Regional.* Air mass trajectory (AMT) of each synoptic analog was compared to the AMT of the corresponding lockdown day. For each day, trajectory density (log of the occurrence of trajectory endpoints) was calculated over a 0.5°x0.5° grid covering Western-Europe. The distribution of spatial correlation values between each day of LP and each analog day is presented in Fig. S4. Since this distribution is rather spread out, a low threshold at 0.2 (representing 70% of analog days, 16.3 analogs/day on average) was selected in order to

220 remove the worst analog AMT, but also to keep sufficient variability. An example of satisfactory and unsatisfactory analogs is shown in Fig. S5.

Local. A specific constrain on local ambient temperature and Relative Humidity (RH) was implemented. Indeed, both variables are key drivers of the partitioning of semi-volatile material, such as ammonium nitrate. Therefore, a satisfactory representation of local meteorological conditions by the analogs is needed in order

225 to robustly capture and characterize any change of concentration. Over the study period, the analog performance regarding temperature and RH respectively ranges from -15°C to +15°C, and from -36% to +64%. Concretely, analogs that are much colder and wetter than the observation day may be associated to enhanced condensation of semi-volatile compounds, which would lead to an overestimation of the estimated decrease of e.g. nitrate. This specifically occurred on April 21st, 22nd and 23rd 2020. To avoid that issue, we excluded

230 from the list the analogs having the 5% worst performance. Acceptable ranges were therefore]-9.3, 6[and]-19, 35[for temperature and RH, respectively. Despite these relatively wide ranges, the A^{3}Q methodology allows to efficiently reconstruct meteorological conditions during the lockdown period. Indeed, Mean Bias of -0.17 m/s, -1.52°C, -1.3 hPa and 8.7% were respectively obtained for wind speed, ambient temperature, pressure and relative humidity, indicating a satisfactory analogy. Sensitivity tests presented below also

235 demonstrate that stricter ranges do not significantly change the analog results.

3.2.2. Data preparation

Daily averages have been computed for each variable. A valid average is considered if at least 75% of the day is covered.

240 Because the dataset consists in multi-year observations, long-term trends may impact the estimated concentration change due to lockdown. To that end, a seasonal Mann-Kendall test was performed on each variable on the 01/2012-02/2020 period. The Mann-Kendall R package was used (Collaud Coen et al., 2020), which includes three pre-whitening approaches in order to reduce the weight of autocorrelation. Results are summarized in Table 1. From this analysis, NO_x, OA, HOA, OOA, O_3, BC_{ff} concentrations (2012-2020, including

245 lockdown) were linearly corrected on a daily basis.

Variable	Sen's slope ($\mu g/m^3$/year)	MK p-value (95% confidence interval)
NO_x	−0.156	0.009
NO_3	−0.037	0.22
SO_4	–	–
OA	−0.068	<0.001
HOA	−0.019	0.049
BBOA	−0.004	0.18
OOA	−0.068	<0.001
O_3	0.459	0.01
PM_1	–	–
BC_{wb}	−0.002	0.067
BC_{ff}	−0.018	<0.001

Table 1. Sen's slope (in $\mu g/m^3$/year) and MK p-value for each variable of the study. No slope means that the result doesn't reach the 95% confidence interval. Slope is statistically significant for p < 0.05.

250 In order to limit the unwanted weight of positive outliers which have poor statistically representativity, the 1% highest daily concentrations of each variable were removed.

3.2.4. Sensitivity tests

The results presented here primarily depend on the list of analog days that is calculated. The overall analog

255 number is at first determined by the strictness of the correlation coefficients of atmospheric circulation and air mass origin. Selection of best analogy leads to poor statistical representativeness (Fig. S6), with a low number of analog days. It is instead preferable to remove analog days associated with worst trajectory correlation (Fig. S4). It is noteworthy that little change in the correlation coefficients (Table 2, Scenario 1-4) has little impact on the results (for all variables) presented in this manuscript (Fig. S7). This can be mainly

260 related to the reasonable change in the number of analog days.

Similarly, the impact of subsequent filtering with temperature and relative humidity were also investigated. To this end, two additionnal scenarios were considered (S5-6, Table 2). S5 and S6 have limited impact on traffic-related variables (Fig. S7), on the contrary to wood-burning tracers and secondary compounds. This especially highlights the essential role of meteorological representativeness in order to characterize the

265 changes of secondary pollution. Indeed, when no temperature and RH filtering is performed (Scenario 5), highest decrease of NO_3 is linked to analog days that are associated to higher RH (Fig. S8a) and lower temperature (Fig. S8b), which favor the partitioning of nitrate in the particulate phase. Scenario 6 has a stricter filtering than the Base one, and exhibits very good performance regarding the reconstruction of

meteorological conditions (Table 3). However, we show that both scenarios have very similar daily NO_3
270 concentration change despite slight discrepancies in meteorological performance. This underlines that the
thresholds used in the Base scenario are sufficient to provide robust results.

	Synoptic analog R	Trajectory analog R	RH acceptability range	T acceptability range	Min. Analog nb
Base	0.6	0.2	]-19, 35[	]-9.3, 6[	5
Scenario 1	0.6	0.3	]-19, 35[	]-9.3, 6[	5
Scenario 2	0.6	0.1	]-19, 35[	]-9.3, 6[	5
Scenario 3	0.5	0.2	]-19, 35[	]-9.3, 6[	5
Scenario 4	0.7	0.2	]-19, 35[	]-9.3, 6[	5
Scenario 5	0.6	0.2	–	–	5
Scenario 6	0.6	0.2	]-19, 17[	]-8, 6[	3

Table 2. Acceptability thresholds used in different scenarios to evaluate the sensitivity of our methodology.

	RH Mean Biais (%)	Temperature Mean Biais (°C)	Wind Speed Mean Biais (m/s)	Pressure Mean Biais (hPa)
Base	-8.7	+1.52	-0.17	-1.3
Scenario 5	-10.5	+2.1	-0.14	-0.52
Scenario 6	-1.95	+1.2	-0.21	-2.35

275 **Table 3. Performance (expressed as Mean Biais) of different scenarios to predict meteorological parameters during
lockdown**

3.2.5. Performance evaluation

Furthermore, the performance of the analog methodology has been evaluated on a business-as-usual period,
280 from 01/01/2020 to 01/03/2020. The construction of the analog list went through the same steps, with the
same thresholds. The acceptability range for T and RH moved to]-5, 4[and]-16, 19[, respectively. This can
be primarily related to the less extreme climatological conditions of Jan.-Feb. 2020. Mean Bias (MB),
Normalised Mean Bias (NMB), Pearson correlation coefficient (r), and the fraction of data within a ratio of 2
(FAC2) have been used for the evaluation.

285 Scatter plots and metric values are respectively presented in Figure 3 and Table 4. Results indicate
satisfactory performance of all variables during the evaluation period, although the range of observed
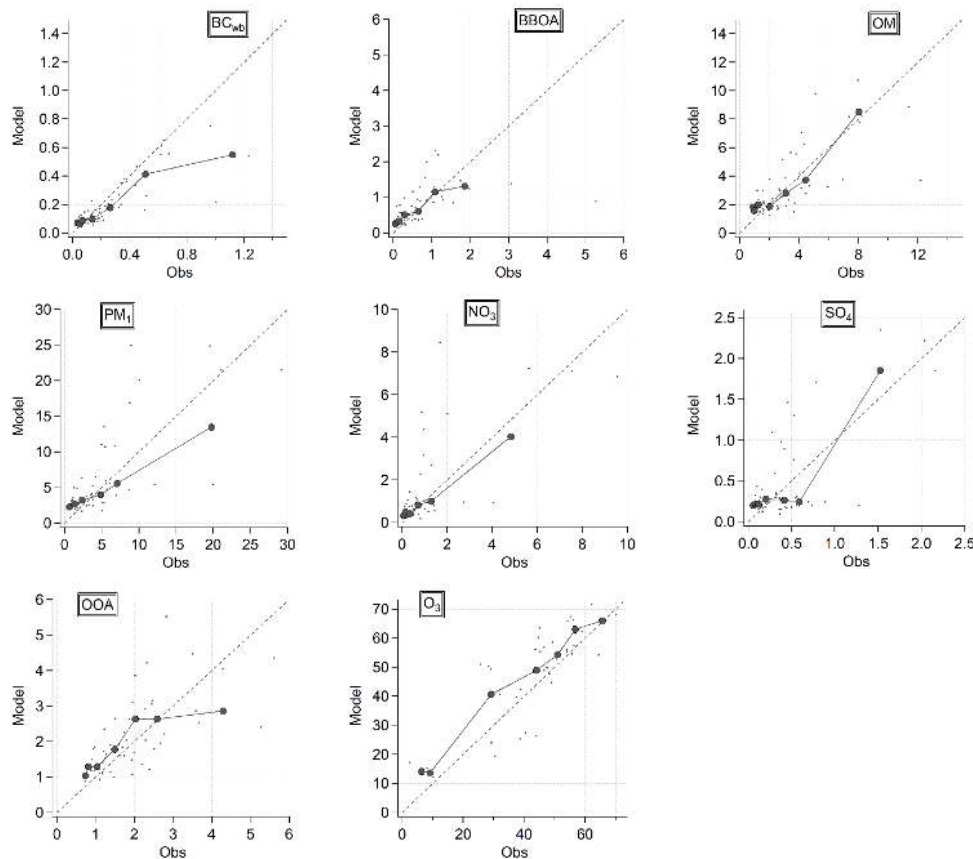concentrations remains rather low.
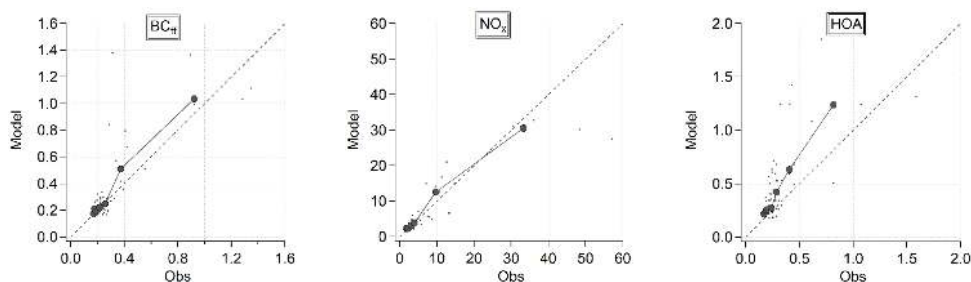
Figure 3. Scatter plots of observed versus estimated concentrations by A³Q during the evaluation period of Jan.-Feb. 2020.

	MB (µg/m³)	NMB (%)	FAC2	R
BC$_{ff}$	0.049	15.3	0.96	0.78
NO$_x$	–0.53	–7.1	0.95	0.90
HOA	0.17	53.0	0.79	0.65
BC$_{wb}$	–0.06	–24.1	0.82	0.82
BBOA	0.04	6.0	0.60	0.45
OM	0.03	0.8	0.93	0.69
PM$_1$	0.89	17.2	0.68	0.73
NO$_3$	0.38	36.1	0.54	0.71
SO$_4$	0.03	7.9	0.46	0.70
OOA	0.19	9.8	0.98	0.63
O$_3$	4.27	9.7	0.95	0.84

Table 4. Metric values (MB, NMB, FAC2 and r) for the evaluation of A³Q during Jan.-Feb. 2020.

4. Results and discussion

295

Figure 4 presents the distribution of absolute concentration change for each specie during lockdown. Results are further discussed in the following subsections.
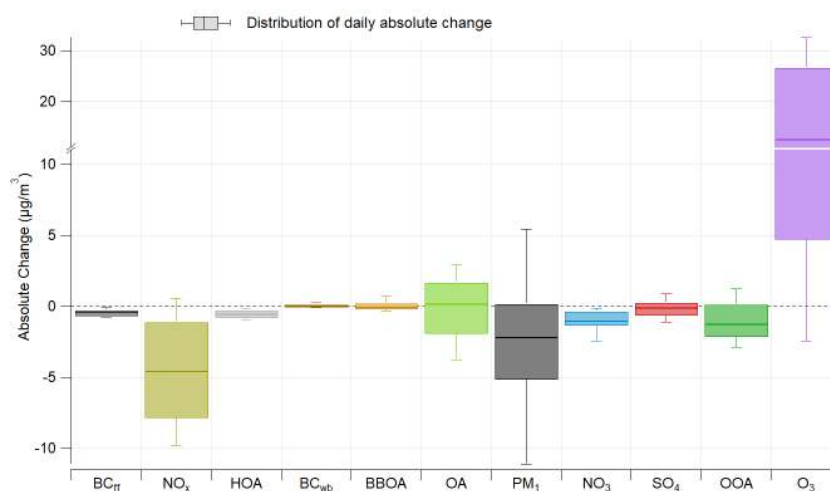
300 **Figure 4: Absolute changes of ambient concentrations of reactive gases and particulate pollutants due to lockdown. Boxplots represent the distribution of daily absolute change (µg/m³); 10th, 25th, 50th, 75th and 90th percentiles were used. Values are presented in Table 5.**

	Absolute change (µg/m³)					Median relative change	p-value
	p10	p25	p50	p75	p90	(%)	
BC_{ff}	-0.74	-0.65	-0.42	-0.28	-0.06	-54.8	3.2×10^{-15}
NO_x	-9.79	-7.81	-4.57	-1.1	0.58	-42.7	2.14×10^{-5}
HOA	-0.98	-0.80	-0.52	-0.27	-0.17	-61.8	1.2×10^{-13}
BC_{wb}	-0.11	-0.03	0.04	0.13	0.24	20.1	0.003
BBOA	-0.36	-0.20	-0.03	0.22	0.72	12.0	0.44
OA	-3.77	-1.89	0.16	1.66	2.95	-6.6	0.71
PM_1	-11.10	-5.13	-2.16	0.17	5.45	-14.9	0.02
NO_3	-2.42	-1.33	-1.03	-0.37	-0.16	-45.5	0.0067
SO_4	-1.14	-0.61	-0.11	0.28	0.90	-10.3	0.21
OOA	-2.92	-2.12	-1.26	0.12	1.21	-25.1	0.002
O_3	-2.49	4.74	12.57	26.70	32.62	20.2	4.45×10^{-9}

Table 5. Distribution of absolute concentration change (10th, 25th, 50th, 75th, 90th percentile has been used), as well as
305 **the median relative change (%). p-values (95% confidence interval) of the pairing Student t-test between Observations and Analog timeseries during lockdown**

4.1. Primary sources

Species usually considered as markers for primary traffic emissions (NO_x, BC_{ff} and HOA) exhibit at
310 SIRTA a median decrease of concentrations by 42-62% (Table 5) at SIRTA. For NO_x, this is very consistent
with previous results in the Paris region using machine learning approaches (-42%, Grange et al., 2020).
Moreover, the NO_x decrease at SIRTA, a peri-urban background station, also matches the relative decrease
calculated for urban and peri-urban stations across the region (-42% and -39%, respectively), although
absolute changes are graduated (-11 $\mu g/m^3$ and -16.4 $\mu g/m^3$ for urban and peri-urban stations, respectively).
315 Although the intensity of the decrease has differed from site to site, the temporality of the change was
uniform at the regional scale, including SIRTA (Fig. 5). It is also consistent with traffic counting data in the
Paris region (https://dataviz.cerema.fr/trafic-routier/), with a slow traffic increase throughout the
lockdown period.
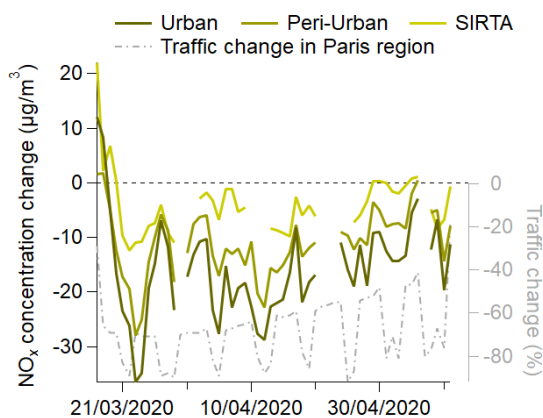
320

Figure 5: Temporal variation of NO_x concentration changes at SIRTA, and urban and periurban background stations of the Paris region.

On the other hand, wood burning tracers (BC_{wb} and BBOA) exhibit an increase of +20% and +58%
325 respectively, which can be primarily related to the stay-at-home order, enhancing emissions of residential
heating (Grange et al., 2020). Although absolute change is limited (Fig.4), by converting BC_{wb} to PM_{wb}, and BC_{ff}
to PM_{ff}, increased PM_{wb} concentrations compensated or even exceeded the decrease of PM_{ff} during specific
days (Fig. 6). At the same time, the mean weekly variation of wood burning changed during lockdown (Fig.
S9), with increased concentrations during the week, compared to the relatively flat variation in business-as-
330 usual conditions (e.g. +67% on Fridays). Therefore, lockdown changed both intensity and temporality of the
wood burning source in the Paris region.

Atmospheric
Chemistry
and Physics
Discussions
Open Access
EGU
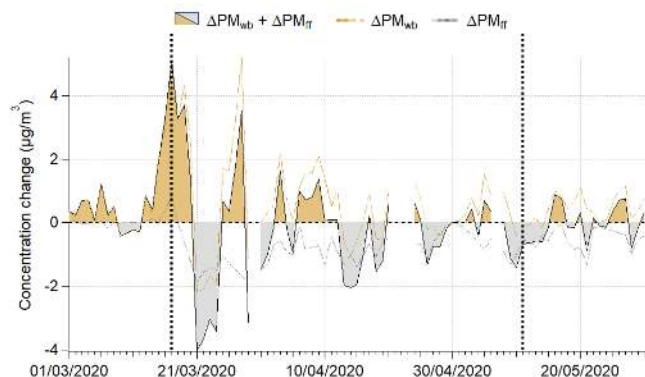
Figure 6 Temporal variations of ΔPM_{wb} + ΔPM_{ff} during lockdown. Brown shaded area shows compensation of wood burning. Individual PM_{wb} and PM_{ff} concentration change are also displayed with dotted lines. Black vertical lines
335 **delimit the start and the end of the lockdown period.**

4.2. NO_x-induced influence on secondary pollutants

   4.2.1. Ozone

Nitrogen oxides play a central role within the atmospheric reactor, enabling the formation of secondary
340   pollutants (Kroll et al., 2020) such as tropospheric ozone and secondary organic and inorganic aerosols (SOA
and SIA, respectively). Ozone is found to increase by 20% (Fig. 4). This negative feedback, due to the titration
effect of NO, is already well characterized (Reis et al., 2000), and the magnitude of the change inversely
follows well the one of NO_x (Fig. 7a). A sharp-enough decrease of NO_x shall tip over ozone formation to a NO_x-
limited system (Markakis et al., 2014), which may be seen from this relationship, where ozone concentration
345   change stabilizes at +20 µg/m³ for ΔNO_x below -10 µg/m³ at SIRTA. Nevertheless, it is worth highlighting
that the climatological extreme of Spring 2020, with strong positive temperature anomalies, should have also
contributed to increased O_3 concentrations, as previously emphasized for Europe (Meleux et al., 2007). Even
though meteorology is taken into account by the A³Q method, the unique character of this springtime
heatwave inherently blurs the discrimination between ambient temperature and NO_x impacts on ozone
350   formation. This limitation would also occur for any other statistical approaches, such as machine learning.
Figure 7b shows indeed that some of the highest ΔO_3 values are associated to high temperatures (daily
average > 18°C), concomitantly with substantial decrease of NO_x concentrations. On the other hand, positive
ΔO_3 are also obtained for rather low temperature (< 10°C) and highest decreases of NO_x, which means that in
this case the increase of O_3 shall be only NO_x-related.

355
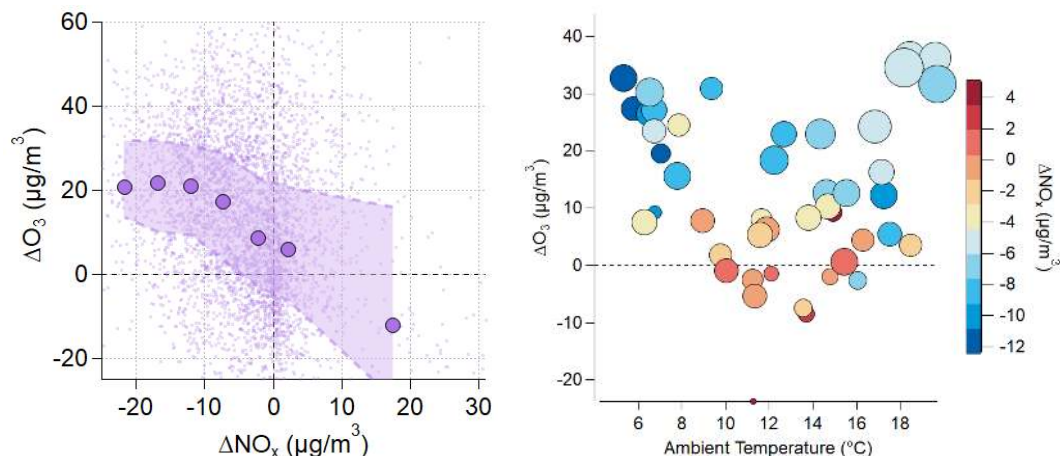
Figure 7 a) Concentration change (µg/m³) of O₃ versus concentration change of NOₓ (µg/m³). Coloured dots correspond to a 100 resampling following the inverse normal distribution law, whose mid-height width is the standard deviation of each analog day. Markers represent the median, bottom and top and shaded area the 25th and 75th percentile, respectively. b) Concentration change of O₃ versus ambient temperature. Marker's color and size are respectively function of ΔNOₓ and observed O₃ concentrations.

4.2.2. Particulate Nitrate

Springtime in the Paris region is usually associated with PM pollution episodes that are mainly triggered by particulate ammonium nitrate (Beekmann et al., 2015) (NH_4NO_3), resulting from the reaction between HNO_3 (NO_x oxidation) and ammonia (NH_3). For that matter, agricultural activities (the major source of NH_3 in Western-Europe (Fortems-Cheiney et al., 2016)) were neither stopped nor restrained during lockdown. Therefore, business-as-usual ammonia concentrations can reasonably be assumed, and since the formation regime of nitrate in Paris has previously been found to be NO_x-limited (Petetin et al., 2016), a change of regime to NH_3-limited is highly unlikely (Viatte et al., 2021). On median, nitrate decreases by 45%. The decrease linearly follows the one of NO_x (Fig. 8), although both compounds differ in terms of reactivity and footprint. A similar relationship is shown when using urban and peri-urban NO_x concentrations (Fig. S10), which is consistent with the temporal correlation of ΔNO_x throughout the Paris region (Fig. 5). However, a slight shouldering of the decrease for urban NO_x can be noticed, which implies that this efficiency regarding NO_3 is related to the amplitude of NO_x reduction.
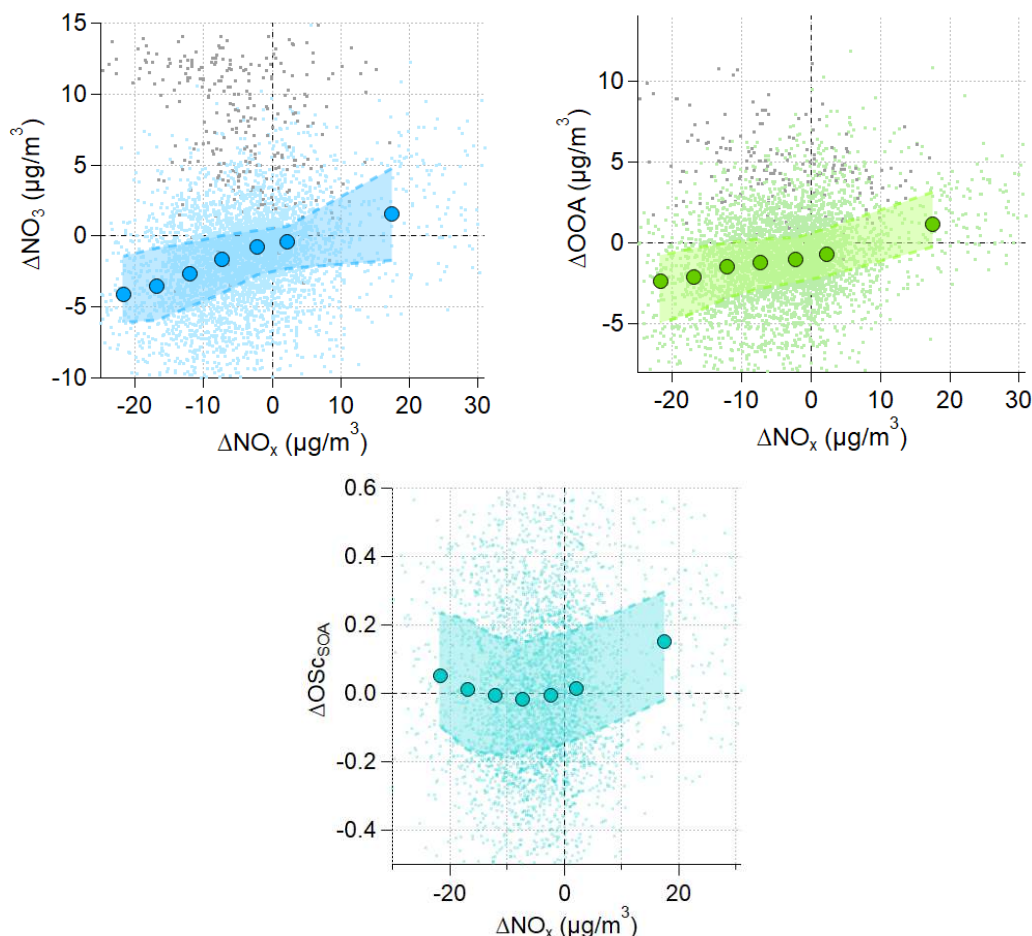
Figure 8 Same as Fig.8a, for NO₃, OOA and OSc$_{SOA}$. Grey dots correspond to days with predominant long–range transport, identified by a positive NO₃ and OOA concentration change concomitantly with a SO₄ concentration peak (Fig. 10), which have been excluded from percentile calculations. Markers represent the median, bottom and top and shaded area the 25th and 75th percentile, respectively.

This result suggests the importance of rapid ammonium nitrate formation at a rather local scale (Petit et al., 2015; Wang et al., 2020), but shall not eclipse continental advection that can occur in Paris, especially during Springtime (e.g. Beekmann et al., 2015). To that end, sulphate shows little change (-8%) with no clear statistical significance ($p>0.05$), which indicates a similar influence of long-range pollution advection, and that SO_2 sources in Eastern Europe (Pay et al., 2012) may not have experienced a significant decrease. Consistent information on that matter are unfortunately still rather scarce at the European scale. Filonchyk et al. (2020) recently showed an increase of SO_2 in several Polish urban areas, although their methodology does not take meteorology into account. The Carbon Monitor initiative (Liu et al., 2020b) also records a decrease of 11.5% of the Power sector in Europe during 2020 compared to 2019. On specific days, positive peaks of ΔNO_3 are concomitant to higher SO_4 concentrations (Fig. 9), which means that nitrate was in these cases mainly advected from long-range transport, despite a decrease of NO_x. It is also concomitant with a higher Nitrogen Oxidation Ratio ($NOR=NO_3/(NO_2+NO_3)$) values, and highest positive change (top panel of Fig. 9). Given the

Atmospheric
Chemistry
and Physics
Discussions
Open Access
EGU

395 NO_x/NO_3 relationship (Fig. 8a), and hypothesizing that a decrease of locally-formed NO_3 is always associated to a decrease of NO_x concentration at the measurement site, long-range transported NO_3 can be assumed to overcompensate the regional decrease. For instance, on March 28th and April 19th, the total ΔNO_3 respectively of 11.7 and 6.7 µg/m^3 could be apportioned into a regional decrease of -5.5 and -3.7 µg/m^3, with an advected contribution of 17.2 and 10.4 µg/m^3, respectively.

400
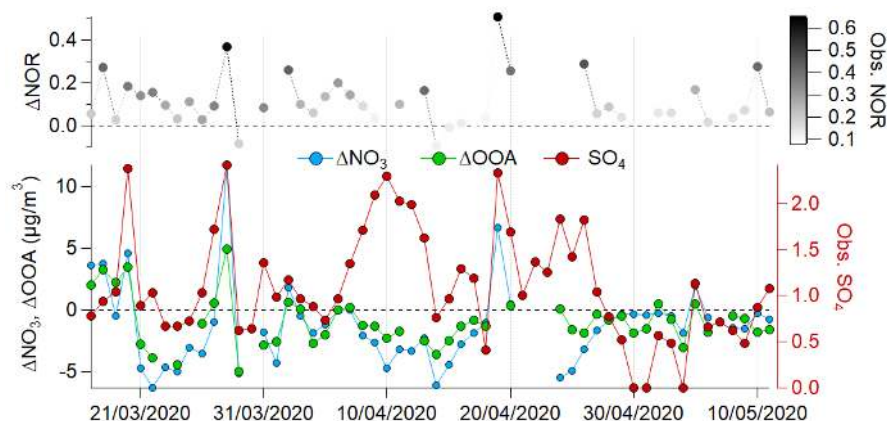
Figure 9 Temporal variation during LP2020 of (bottom) ΔNO_3, ΔOOA and SO_4 concentrations (µg/m^3); (top) ΔNOR
405 **values, color-coded by observed NOR.**

4.2.3. Secondary Organic Aerosols

Secondary organic aerosols, proxied by OOA concentrations, exhibit a decrease of 25% compared to
410 business-as-usual conditions. Given the multitude of SOA precursors and formation pathways, this decrease can be linked to numerous factors. Indeed, Srivastava et al. (2019) recently highlighted the complexity of the SOA fractions in the Paris region during Springtime. The lack of specific organic tracers prevents from thoroughly apportioning SOA over the long-term analysis period of 2012-2020. As a consequence, the apparent decrease of 25% may derive from several compensatory feedbacks, which cannot be individually
415 characterized here. Although SOA in Paris can't be only related to traffic (Crippa et al., 2013; Srivastava et al., 2019), the decrease of OOA seems to be also correlated with ΔNO_x (Figure 8b). NO_x steps in SOA formation notably when reacting with peroxy radicals (R-O_2), resulting from VOCs oxidation with the hydroxyl radical. The exceptional amount of sunshine during lockdown may have positively influenced the availability of OH$^\bullet$ for the initialization of SOA formation. However, no direct observations available at SIRTA can support this
420 assumption directly. The odd oxygen O_x (= O_3 + NO_2), a conservative tracer of photochemical chemistry (Sun et al., 2020), shows a slight increase (+9%). But unlike the findings of Herndon et al. (2008) in Mexico-city during Spring, only a moderate correlation is found with OOA (r^2=0.4, slope = 0.068, following the

recommendation of removing wood-burning and long range transport related episodes). This may be linked to the rather low O_x concentrations (60-110μg/m^3) during the lockdown period.

425   Despite very limited change on average (<1%), daily OSc_{SOA} is found to differ from business as usual conditions, adopting a comma-like shape, function of ΔNO_x (Fig. 8c). Indeed, although ΔOSc_{SOA} decreases until $\Delta NO_x > -7$ μg/m^3, it increases back for higher NO_x decreases, reaching a median of +0.05. Despite being moderate, this behaviour may reflect some changes in SOA chemistry, notably regarding gas-phase oxidation of anthropogenic precursors, as highlighted in Herndon et al. (2008). But at this stage, the whole equation
430   comprises too many unknown variables (from VOC precursors to particulate end products) in order to fully describe the impacts of lockdown measures onto the numourous SOA formation mechanismsremains arduously apprehendable.

435   **4.3. Implications for air quality**

The lockdown enforced during Spring 2020 in Paris corresponds to a real-life emission scenario, representing the extreme case of a quasi-total interruption of the vehicular traffic source. Up to now, no mitigation policy could have gone that far. From the results presented here, the impact of NO_x control on submicron primary traffic-related aerosols (BC_{ff} and HOA) remains limited, mainly because both don't
440   contribute much to PM$_1$ concentrations during Spring (5.0 and 5.7% respectively). However, it is worth mentioning that a higher impact can be expected within PM$_{10}$ in the vicinity of traffic, related to the decrease of non-exhaust emissions (brake/tire wear and resuspension). This fraction has recently been highlighted as particularly harmful for human health (Daellenbach et al., 2020); therefore NO_x control shall provide a significant co-benefit for that specific matter.

445   Reducing the concentrations of secondary compounds is an arduous task, because mitigation policies can inherently only focus on the reduction of primary pollutants. But regional NO_x reduction appears to have the potential to be an efficient mitigation policy regarding secondary aerosols (mainly NO$_3$ and SOA to a lesser extent), which account on average for more than half of PM$_1$ during Spring at SIRTA (respectively 28.9% and 31.4%). Moreover, although the traffic ban has been applied consistently over the lockdown period, the
450   decrease of NO_x concentrations at SIRTA ranges from 0 to around -20 μg/m^3. Adding the impact of NO_x on BC_{ff}, HOA, NO$_3$, NH$_4$ (considering neutralized aerosols) and OOA together, the corresponding change of PM-related material ranges from -2 to -9 μg/m^3 (Fig. 10). The efficiency of NO_x mitigation shall therefore be put in perspective with meteorological conditions (e.g. horizontal dispersion, since lowest ΔNO_x values are associated to continental air masses), as well as the vertical atmospheric dynamic (Dupont et al., 2016). It is
455   also worth mentioning that in the case of long-range pollution transport episodes, substantial efforts to reduce emissions at the city scale will not be enough to counterbalance additional advected material, as shown previously for NO$_3$ and OOA.
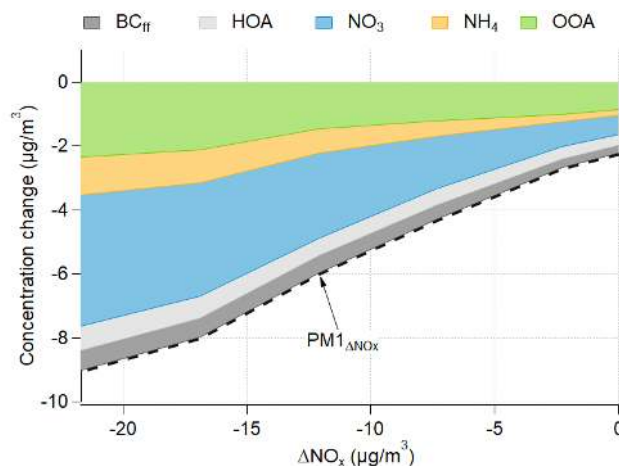
Figure 10 Impact of regional NO$_x$ concentration change on PM-related species (BC$_{ff}$, HOA, NO$_3$, NH$_4$, OOA). ΔNH$_4$ was estimated from ΔNO$_3$, assuming aerosol neutralization (Petit et al., 2015).

5. Conclusion

The COVID-19 pandemic led to life-changing restrictions, with strict stay-at-home orders in Western-Europe during Spring 2020. As a consequence, light-duty vehicular traffic was almost completely stopped in urban areas, such as the Paris region. Despite tragic death records, lockdowns represent an open-air mitigation experiment, in a period that is usually associated with PM pollution episodes dominated by secondary material. However, the characterization of a change in chemical composition is not straightforward because meteorology can strongly contribute to the temporal variability of atmospheric pollutants. To that end, a unique methodology was built in order to compare each day of lockdown with analog days, having similar meteorology. The analogy was based on three successive meteorological layers, where synoptic, regional and local meteorology was considered. This innovative approach was applied to a comprehensive in-situ dataset, acquired at the SIRTA observatory, a sub-urban station located 20km South-West of Paris. The A^{3}Q method provided very satisfactory results over a business-as-usual period, which ensures a robust characterization of concentration changes in the Paris region during lockdown.

The unprecedented drop of traffic commuting due to the stay-at-home order led to an expected decrease of primary traffic pollutants, NO$_x$ (-42%), HOA (-62%) and BC$_{ff}$ (-55%), as well as an increase of ozone concentrations due to the lesser contribution of the O3 sink by NO. Concomitantly, primary particles related to residential wood-burning shows a slight increase (+ 12-20%). The decrease of NO$_x$ (-42%) triggered positive feedbacks regarding secondary aerosols especially nitrate and SOA, which are found to drop by 42% and 25% respectively. A NO$_x$ relationship suggests the significance of rather local pollution formation, contrasting with previous results in the region. The decrease of NO$_3$ was compensated sporadically during long-range transport episodes. Oxidation state of SOA is also seen to vary with NO$_x$ concentration change, but our understanding of the involved phenomena still remains limited, notably due to the lack of long-term VOC in-situ observations in the Paris region.

Atmospheric
Chemistry
and Physics
Discussions

Finally, the proposed A³Q method may be considered as an efficient tool to monitor and quantify more precisely the impact of lockdowns in other urban areas. It could also be useful for the quantitative evaluation of emergency mitigation policies settled during pollution episodes.

490

495

520

525

Atmospheric
Chemistry
and Physics
Discussions

References

Adams, M. D.: Air pollution in Ontario, Canada during the COVID-19 State of Emergency, Science of The Total Environment, 742, 140516, https://doi.org/10.1016/j.scitotenv.2020.140516, 2020.

530 Aiken, A. C., DeCarlo, P. F., Kroll, J. H., Worsnop, D. R., Huffman, J. A., Docherty, K. S., Ulbrich, I. M., Mohr, C., Kimmel, J. R., and Sueper, D.: O/C and OM/OC ratios of primary, secondary, and ambient organic aerosols with high-resolution time-of-flight aerosol mass spectrometry, 42, 4478–4485, 2008.

Anderson, R. M., Heesterbeek, H., Klinkenberg, D., and Hollingsworth, T. D.: How will country-based mitigation measures influence the course of the COVID-19 epidemic?, The Lancet, 395, 931–934, https://doi.org/10.1016/S0140-6736(20)30567-5, 2020.

535 Beekmann, M., Prévôt, A. S. H., Drewnick, F., Sciare, J., Pandis, S. N., Denier van der Gon, H. A. C., Crippa, M., Freutel, F., Poulain, L., Ghersi, V., Rodriguez, E., Beirle, S., Zotter, P., von der Weiden-Reinmüller, S.-L., Bressi, M., Fountoukis, C., Petetin, H., Szidat, S., Schneider, J., Rosso, A., El Haddad, I., Megaritis, A., Zhang, Q. J., Michoud, V., Slowik, J. G., Moukhtar, S., Kolmonen, P., Stohl, A., Eckhardt, S., Borbon, A., Gros, V., Marchand, N., Jaffrezo, J. L., Schwarzenboeck, A., Colomb, A., Wiedensohler, A., Borrmann, S., Lawrence, M., Baklanov, A., and Baltensperger, U.: In situ, satellite
540 measurement and model evidence on the dominant regional contribution to fine particulate matter levels in the Paris megacity, 15, 9577–9591, https://doi.org/10.5194/acp-15-9577-2015, 2015.

Budisulistiorini, S. H., Canagaratna, M. R., Croteau, P. L., Baumann, K., Edgerton, E. S., Kollman, M. S., Ng, N. L., Verma, V., Shaw, S. L., Knipping, E. M., Worsnop, D. R., Jayne, J. T., Weber, R. J., and Surratt, J. D.: Intercomparison of an Aerosol Chemical Speciation Monitor (ACSM) with ambient fine aerosol measurements in downtown Atlanta, Georgia, 7, 1929–1941,
545 https://doi.org/10.5194/amt-7-1929-2014, 2014.

Canagaratna, M. R., Jimenez, J. L., Kroll, J. H., Chen, Q., Kessler, S. H., Massoli, P., Hildebrandt Ruiz, L., Fortner, E., Williams, L. R., Wilson, K. R., Surratt, J. D., Donahue, N. M., Jayne, J. T., and Worsnop, D. R.: Elemental ratio measurements of organic compounds using aerosol mass spectrometry: characterization, improved calibration, and implications, 14, 19791–19835, https://doi.org/10.5194/acpd-14-19791-2014, 2014.

550 Canonaco, F., Crippa, M., Slowik, J. G., Baltensperger, U., and Prévôt, A. S. H.: SoFi, an IGOR-based interface for the efficient use of the generalized multilinear engine (ME-2) for the source apportionment: ME-2 application to aerosol mass spectrometer data, 6, 3649–3661, https://doi.org/10.5194/amt-6-3649-2013, 2013.

Canonaco, F., Slowik, J. G., Baltensperger, U., and Prévôt, A. S. H.: Seasonal differences in oxygenated organic aerosol composition: implications for emissions sources and factor analysis, 15, 6993–7002, https://doi.org/10.5194/acp-15-6993-
555 2015, 2015.

Canonaco, F., Tobler, A., Chen, G., Sosedova, Y., Slowik, J. G., Bozzetti, C., Daellenbach, K. R., ElHaddad, I., Crippa, M., Huang, R.-J., Furger, M., Baltensperger, U., and Prévôt, A. S. H.: A new method for long-term source apportionment with time-dependent factor profiles and uncertainty assessment using SoFi Pro: application to one year of organic aerosol data, https://doi.org/10.5194/amt-2020-204, 2020.

560 Cattiaux, J., Yiou, P., and Vautard, R.: Dynamics of future seasonal temperature trends and extremes in Europe: a multi-model analysis from CMIP3, Climate Dynamics, 38, 1949–1964, https://doi.org/10.1007/s00382-011-1211-1, 2012.

Chiriaco, M., Dupont, J.-C., Bastin, S., Badosa, J., Lopez, J., Haeffelin, M., Chepfer, H., and Guzman, R.: ReOBS: a new approach to synthesize long-term multi-variable dataset and application to the SIRTA supersite, Earth Syst. Sci. Data, 10, 919–940, https://doi.org/10.5194/essd-10-919-2018, 2018.

565 Collaud Coen, M., Andrews, E., Bigi, A., Martucci, G., Romanens, G., Vogt, F. P. A., and Vuilleumier, L.: Effects of the prewhitening method, the time granularity, and the time segmentation on the Mann–Kendall trend detection and the associated Sen's slope, Atmos. Meas. Tech., 13, 6945–6964, https://doi.org/10.5194/amt-13-6945-2020, 2020.

Crenn, V., Sciare, J., Croteau, P. L., Verlhac, S., Fröhlich, R., Belis, C. A., Aas, W., Äijälä, M., Alastuey, A., Artiñano, B., Baisnée, D., Bonnaire, N., Bressi, M., Canagaratna, M., Canonaco, F., Carbone, C., Cavalli, F., Coz, E., Cubison, M. J., Esser-
570 Gietl, J. K., Green, D. C., Gros, V., Heikkinen, L., Herrmann, H., Lunder, C., Minguillón, M. C., Močnik, G., O'Dowd, C. D., Ovadnevaite, J., Petit, J.-E., Petralia, E., Poulain, L., Priestman, M., Riffault, V., Ripoll, A., Sarda-Estève, R., Slowik, J. G., Setyan, A., Wiedensohler, A., Baltensperger, U., Prévôt, A. S. H., Jayne, J. T., and Favez, O.: ACTRIS ACSM intercomparison – Part 1: Reproducibility of concentration and fragment results from 13 individual Quadrupole Aerosol Chemical Speciation Monitors (Q-ACSM) and consistency with co-located instruments, 8, 5063–5087, https://doi.org/10.5194/amt-8-5063-2015,
575 2015.

Crippa, M., Canonaco, F., Slowik, J. G., El Haddad, I., DeCarlo, P. F., Mohr, C., Heringa, M. F., Chirico, R., Marchand, N., Temime-Roussel, B., Abidi, E., Poulain, L., Wiedensohler, A., Baltensperger, U., and Prévôt, A. S. H.: Primary and secondary organic aerosol origin by combined gas-particle phase source apportionment, Atmos. Chem. Phys., 13, 8411–8426, https://doi.org/10.5194/acp-13-8411-2013, 2013.

580 Daellenbach, K. R., Uzu, G., Jiang, J., Cassagnes, L.-E., Leni, Z., Vlachou, A., Stefenelli, G., Canonaco, F., Weber, S., Segers, A., Kuenen, J. J. P., Schaap, M., Favez, O., Albinet, A., Aksoyoglu, S., Dommen, J., Baltensperger, U., Geiser, M., El Haddad, I., Jaffrezo, J.-L., and Prévôt, A. S. H.: Sources of particulate-matter air pollution and its oxidative potential in Europe, Nature, 587, 414–419, https://doi.org/10.1038/s41586-020-2902-8, 2020.

Dantas, G., Siciliano, B., França, B. B., da Silva, C. M., and Arbilla, G.: The impact of COVID-19 partial lockdown on the air 585 quality of the city of Rio de Janeiro, Brazil, Science of The Total Environment, 729, 139085, https://doi.org/10.1016/j.scitotenv.2020.139085, 2020.

Drinovec, L., Močnik, G., Zotter, P., Prévôt, A. S. H., Ruckstuhl, C., Coz, E., Rupakheti, M., Sciare, J., Müller, T., Wiedensohler, A., and Hansen, A. D. A.: The "dual-spot" Aethalometer: an improved measurement of aerosol black carbon with real-time loading compensation, 8, 1965–1979, https://doi.org/10.5194/amt-8-1965-2015, 2015.

590 Dupont, J.-C., Haeffelin, M., Badosa, J., Elias, T., Favez, O., Petit, J. E., Meleux, F., Sciare, J., Crenn, V., and Bonne, J. L.: Role of the boundary layer dynamics effects on an extreme air pollution event in Paris, 141, 571–579, https://doi.org/10.1016/j.atmosenv.2016.06.061, 2016.

Filonchyk, M., Hurynovich, V., and Yan, H.: Impact of Covid-19 lockdown on air quality in the Poland, Eastern Europe, Environmental Research, 110454, https://doi.org/10.1016/j.envres.2020.110454, 2020.

595 Fortems-Cheiney, A., Dufour, G., Hamaoui-Laguel, L., Foret, G., Siour, G., Van Damme, M., Meleux, F., Coheur, P.-F., Clerbaux, C., Clarisse, L., Favez, O., Wallasch, M., and Beekmann, M.: Unaccounted variability in NH3 agricultural sources detected by IASI contributing to European spring haze episode: Agricultural NH3 Detected by IASI, 43, 5475–5482, https://doi.org/10.1002/2016GL069361, 2016.

Freney, E., Zhang, Y., Croteau, P., Amodeo, T., Williams, L., Truong, F., Petit, J.-E., Sciare, J., Sarda-Esteve, R., Bonnaire, 600 N., Arumae, T., Aurela, M., Bougiatioti, A., Mihalopoulos, N., Coz, E., Artinano, B., Crenn, V., Elste, T., Heikkinen, L., Poulain, L., Wiedensohler, A., Herrmann, H., Priestman, M., Alastuey, A., Stavroulas, I., Tobler, A., Vasilescu, J., Zanca, N., Canagaratna, M., Carbone, C., Flentje, H., Green, D., Maasikmets, M., Marmureanu, L., Minguillon, M. C., Prevot, A. S. H., Gros, V., Jayne, J., and Favez, O.: The second ACTRIS inter-comparison (2016) for Aerosol Chemical Speciation Monitors (ACSM): Calibration protocols and instrument performance evaluations, Aerosol Science and Technology, 53, 830–842, 605 https://doi.org/10.1080/02786826.2019.1608901, 2019.

Grange, S. K., Lee, J. D., Drysdale, W. S., Lewis, A. C., Hueglin, C., Emmenegger, L., and Carslaw, D. C.: COVID-19 lockdowns highlight a risk of increasing ozone pollutionin European urban areas, https://doi.org/10.5194/acp-2020-1171, 2020.

Haeffelin, M., Barthès, L., Bock, O., Boitel, C., Bony, S., Bouniol, D., Chepfer, H., Chiriaco, M., Cuesta, J., and Delanoë, J.: 610 SIRTA, a ground-based atmospheric observatory for cloud and aerosol research, 253–275, 2005.

Herndon, S. C., Onasch, T. B., Wood, E. C., Kroll, J. H., Canagaratna, M. R., Jayne, J. T., Zavala, M. A., Knighton, W. B., Mazzoleni, C., Dubey, M. K., Ulbrich, I. M., Jimenez, J. L., Seila, R., de Gouw, J. A., de Foy, B., Fast, J., Molina, L. T., Kolb, C. E., and Worsnop, D. R.: Correlation of secondary organic aerosol with odd oxygen in Mexico City, Geophys. Res. Lett., 35, L15804, https://doi.org/10.1029/2008GL034058, 2008.

615 Kalnay, E., Kanamitsu, M., Kistler, R., Collins, W., Deaven, D., Gandin, L., Iredell, M., Saha, S., White, G., Woollen, J., Zhu, Y., Leetmaa, A., Reynolds, B., Chelliah, M., Ebisuzaki, W., Higgins, W., Janowiak, J., Mo, K. C., Ropelewski, C., Wang, J., Jenne, R., and Joseph, D.: The NCEP/NCAR 40-Year Reanalysis Project., 77, 437–472, https://doi.org/10.1175/1520-0477(1996)077<0437:TNYRP>2.0.CO;2, 1996.

Kroll, J. H., Donahue, N. M., Jimenez, J. L., Kessler, S. H., Canagaratna, M. R., Wilson, K. R., Altieri, K. E., Mazzoleni, L. 620 R., Wozniak, A. S., Bluhm, H., Mysak, E. R., Smith, J. D., Kolb, C. E., and Worsnop, D. R.: Carbon oxidation state as a metric for describing the chemistry of atmospheric organic aerosol, 3, 133–139, https://doi.org/10.1038/nchem.948, 2011.

Kroll, J. H., Heald, C. L., Cappa, C. D., Farmer, D. K., Fry, J. L., Murphy, J. G., and Steiner, A. L.: The complex chemical effects of COVID-19 shutdowns on air quality, Nat. Chem., 12, 777–779, https://doi.org/10.1038/s41557-020-0535-z, 2020.

Le, T., Wang, Y., Liu, L., Yang, J., Yung, Y. L., Li, G., and Seinfeld, J. H.: Unexpected air pollution with marked emission 625 reductions during the COVID-19 outbreak in China, Science, eabb7431, https://doi.org/10.1126/science.abb7431, 2020.

Liu, Q., Harris, J. T., Chiu, L. S., Sun, D., Houser, P. R., Yu, M., Duffy, D. Q., Little, M. M., and Yang, C.: Spatiotemporal impacts of COVID-19 on air pollution in California, USA, Science of The Total Environment, 141592, https://doi.org/10.1016/j.scitotenv.2020.141592, 2020a.

630   Liu, Z., Ciais, P., Deng, Z., Davis, S. J., Zheng, B., Wang, Y., Cui, D., Zhu, B., Dou, X., Ke, P., Sun, T., Guo, R., Zhong, H., Boucher, O., Bréon, F.-M., Lu, C., Guo, R., Xue, J., Boucher, E., Tanaka, K., and Chevallier, F.: Carbon Monitor, a near-real-time daily dataset of global CO2 emission from fossil fuel and cement production, Sci Data, 7, 392, https://doi.org/10.1038/s41597-020-00708-7, 2020b.

Lorenz, E. N.: The predictability of a flow which possesses many scales of motion, 21, 289–307, https://doi.org/10.1111/j.2153-3490.1969.tb00444.x, 1969.

635   Mahato, S., Pal, S., and Ghosh, K. G.: Effect of lockdown amid COVID-19 pandemic on air quality of the megacity Delhi, India, Science of The Total Environment, 730, 139086, https://doi.org/10.1016/j.scitotenv.2020.139086, 2020.

Markakis, K., Valari, M., Colette, A., Sanchez, O., Perrussel, O., Honore, C., Vautard, R., Klimont, Z., and Rao, S.: Air quality in the mid-21st century for the city of Paris under two climate scenarios; from the regional to local scale, Atmos. Chem. Phys., 14, 7323–7340, https://doi.org/10.5194/acp-14-7323-2014, 2014.

640   Meleux, F., Solmon, F., and Giorgi, F.: Increase in summer European ozone amounts due to climate change, Atmospheric Environment, 41, 7577–7587, https://doi.org/10.1016/j.atmosenv.2007.05.048, 2007.

Mesas-Carrascosa, F.-J., Pérez Porras, F., Triviño-Tarradas, P., García-Ferrer, A., and Meroño-Larriva, J. E.: Effect of Lockdown Measures on Atmospheric Nitrogen Dioxide during SARS-CoV-2 in Spain, Remote Sensing, 12, 2210, https://doi.org/10.3390/rs12142210, 2020.

645   Middlebrook, A. M., Bahreini, R., Jimenez, J. L., and Canagaratna, M. R.: Evaluation of Composition-Dependent Collection Efficiencies   for   the   Aerodyne   Aerosol   Mass   Spectrometer   using   Field   Data,   46,   258–271, https://doi.org/10.1080/02786826.2011.620041, 2012.

Ng, N. L., Herndon, S. C., Trimborn, A., Canagaratna, M. R., Croteau, P. L., Onasch, T. B., Sueper, D., Worsnop, D. R., Zhang, Q., and Sun, Y. L.: An aerosol chemical speciation monitor (ACSM) for routine monitoring of the composition and 650   mass concentrations of ambient aerosol, 45, 780–794, 2011.

Otmani, A., Benchrif, A., Tahri, M., Bounakhla, M., Chakir, E. M., El Bouch, M., and Krombi, M.: Impact of Covid-19 lockdown on PM10, SO2 and NO2 concentrations in Salé City (Morocco), Science of The Total Environment, 735, 139541, https://doi.org/10.1016/j.scitotenv.2020.139541, 2020.

Paatero, P. and Tapper, U.: Positive matrix factorization: A non-negative factor model with optimal utilization of error 655   estimates of data values, 5, 111–126, https://doi.org/10.1002/env.3170050203, 1994.

Pay, M. T., Jiménez-Guerrero, P., and Baldasano, J. M.: Assessing sensitivity regimes of secondary inorganic aerosol formation in Europe with the CALIOPE-EU modeling system, 51, 146–164, https://doi.org/10.1016/j.atmosenv.2012.01.027, 2012.

Petetin, H., Sciare, J., Bressi, M., Gros, V., Rosso, A., Sanchez, O., Sarda-Estève, R., Petit, J.-E., and Beekmann, M.: Assessing 660   the ammonium nitrate formation regime in the Paris megacity and its representation in the CHIMERE model, 16, 10419–10440, https://doi.org/10.5194/acp-16-10419-2016, 2016.

Petetin, H., Bowdalo, D., Soret, A., Guevara, M., Jorba, O., Serradell, K., and Pérez García-Pando, C.: Meteorology-normalized impact of COVID-19 lockdown upon NO2 pollution in Spain, https://doi.org/10.5194/acp-2020-446, 2020.

Petit, J.-E., Favez, O., Sciare, J., Canonaco, F., Croteau, P., Močnik, G., Jayne, J., Worsnop, D., and Leoz-Garziandia, E.: 665   Submicron aerosol source apportionment of wintertime pollution in Paris, France by double positive matrix factorization (PMF2) using an aerosol chemical speciation monitor (ACSM) and a multi-wavelength Aethalometer, 14, 13773–13787, https://doi.org/10.5194/acp-14-13773-2014, 2014.

Petit, J.-E., Favez, O., Sciare, J., Crenn, V., Sarda-Estève, R., Bonnaire, N., Močnik, G., Dupont, J.-C., Haeffelin, M., and Leoz-Garziandia, E.: Two years of near real-time chemical composition of submicron aerosols in the region of Paris using an 670   Aerosol Chemical Speciation Monitor (ACSM) and a multi-wavelength Aethalometer, 15, 2985–3005, https://doi.org/10.5194/acp-15-2985-2015, 2015.

Petit, J.-E., Favez, O., Albinet, A., and Canonaco, F.: A user-friendly tool for comprehensive evaluation of the geographical origins of atmospheric pollution: Wind and trajectory analyses, 88, 183–187, https://doi.org/10.1016/j.envsoft.2016.11.022, 2017a.

675 Petit, J.-E., Amodeo, T., Meleux, F., Bessagnet, B., Menut, L., Grenier, D., Pellan, Y., Ockler, A., Rocq, B., Gros, V., Sciare, J., and Favez, O.: Characterising an intense PM pollution episode in March 2015 in France from multi-site approach and near real time data: Climatology, variabilities, geographical origins and model evaluation, 155, 68–84, https://doi.org/10.1016/j.atmosenv.2017.02.012, 2017b.

Poulain, L., Spindler, G., Grüner, A., Tuch, T., Stieger, B., van Pinxteren, D., Petit, J.-E., Favez, O., Herrmann, H., and
680 Wiedensohler, A.: Multi-year ACSM measurements at the central European research station Melpitz (Germany) – Part 1: Instrument robustness, quality assurance, and impact of upper size cutoff diameter, Atmos. Meas. Tech., 13, 4973–4994, https://doi.org/10.5194/amt-13-4973-2020, 2020.

Raynaud, D., Hingray, B., Zin, I., Anquetin, S., Debionne, S., and Vautard, R.: Atmospheric analogues for physically consistent scenarios of surface weather in Europe and Maghreb: ATMOSPHERIC ANALOGUES FOR PHYSICALLY CONSISTENT
685 SURFACE WEATHER, Int. J. Climatol., 37, 2160–2176, https://doi.org/10.1002/joc.4844, 2017.

Reis, S., Simpson, D., Friedrich, R., Jonson, J. E., Unger, S., and Obermeier, A.: Road traffic emissions – predictions of future contributions to regional ozone levels in Europe, Atmospheric Environment, 34, 4701–4710, https://doi.org/10.1016/S1352-2310(00)00202-8, 2000.

Sandradewi, J., Prévôt, A. S. H., Szidat, S., Perron, N., Alfarra, M. R., Lanz, V. A., Weingartner, E., and Baltensperger, U.:
690 Using Aerosol Light Absorption Measurements for the Quantitative Determination of Wood Burning and Traffic Emission Contributions to Particulate Matter, 42, 3316–3323, https://doi.org/10.1021/es702253m, 2008.

Sicard, P., De Marco, A., Agathokleous, E., Feng, Z., Xu, X., Paoletti, E., Rodriguez, J. J. D., and Calatayud, V.: Amplified ozone pollution in cities during the COVID-19 lockdown, Science of The Total Environment, 735, 139542, https://doi.org/10.1016/j.scitotenv.2020.139542, 2020.

695 Siciliano, B., Dantas, G., da Silva, C. M., and Arbilla, G.: Increased ozone levels during the COVID-19 lockdown: Analysis for the city of Rio de Janeiro, Brazil, Science of The Total Environment, 737, 139765, https://doi.org/10.1016/j.scitotenv.2020.139765, 2020.

Srivastava, D., Favez, O., Petit, J.-E., Zhang, Y., Sofowote, U. M., Hopke, P. K., Bonnaire, N., Perraudin, E., Gros, V., Villenave, E., and Albinet, A.: Speciation of organic fractions does matter for aerosol source apportionment. Part 3: Combining
700 off-line and on-line measurements, Science of The Total Environment, 690, 944–955, https://doi.org/10.1016/j.scitotenv.2019.06.378, 2019.

Stein, A. F., Draxler, R. R., Rolph, G. D., Stunder, B. J. B., Cohen, M. D., and Ngan, F.: NOAA's HYSPLIT Atmospheric Transport and Dispersion Modeling System, 96, 2059–2077, https://doi.org/10.1175/BAMS-D-14-00110.1, 2015.

Stirnberg, R., Cermak, J., Kotthaus, S., Haeffelin, M., Andersen, H., Fuchs, J., Kim, M., Petit, J.-E., and Favez, O.:
705 Meteorology-driven variability of air pollution (PM1) revealed with explainable machine learning, 30, 2021.

Sun, Y., Lei, L., Zhou, W., Chen, C., He, Y., Sun, J., Li, Z., Xu, W., Wang, Q., Ji, D., Fu, P., Wang, Z., and Worsnop, D. R.: A chemical cocktail during the COVID-19 outbreak in Beijing, China: Insights from six-year aerosol particle composition measurements during the Chinese New Year holiday, Science of The Total Environment, 742, 140739, https://doi.org/10.1016/j.scitotenv.2020.140739, 2020.

710 Toscano, D. and Murena, F.: The Effect on Air Quality of Lockdown Directives to Prevent the Spread of SARS-CoV-2 Pandemic in Campania Region—Italy: Indications for a Sustainable Development, Sustainability, 12, 5558, https://doi.org/10.3390/su12145558, 2020.

Van Den Dool, H. M.: Searching for analogues, how long must we wait?, Tellus A, 46, 314–324, https://doi.org/10.1034/j.1600-0870.1994.t01-2-00006.x, 1994.

715 Vautard, R., Colette, A., van Meijgaard, E., Meleux, F., Jan van Oldenborgh, G., Otto, F., Tobin, I., and Yiou, P.: Attribution of Wintertime Anticyclonic Stagnation Contributing to Air Pollution in Western Europe, 99, S70–S75, https://doi.org/10.1175/BAMS-D-17-0113.1, 2018.

Viatte, C., Petit, J.-E., Yamanouchi, S., Van Damme, M., Doucerain, C., Germain-Piaulenne, E., Gros, V., Favez, O., Clarisse, L., Coheur, P.-F., Strong, K., and Clerbaux, C.: Ammonia and PM2.5 Air Pollution in Paris during the 2020 COVID
720 Lockdown, Atmosphere, 12, 160, https://doi.org/10.3390/atmos12020160, 2021.

Wang, M., Kong, W., Marten, R., He, X.-C., Chen, D., Pfeifer, J., Heitto, A., Kontkanen, J., Dada, L., Kürten, A., Yli-Juuti, T., Manninen, H. E., Amanatidis, S., Amorim, A., Baalbaki, R., Baccarini, A., Bell, D. M., Bertozzi, B., Bräkling, S., Brilke, S., Murillo, L. C., Chiu, R., Chu, B., De Menezes, L.-P., Duplissy, J., Finkenzeller, H., Carracedo, L. G., Granzin, M., Guida, R., Hansel, A., Hofbauer, V., Krechmer, J., Lehtipalo, K., Lamkaddam, H., Lampimäki, M., Lee, C. P., Makhmutov, V., Marie, G., Mathot, S., Mauldin, R. L., Mentler, B., Müller, T., Onnela, A., Partoll, E., Petäjä, T., Philippov, M., Pospisilova, V., Ranjithkumar, A., Rissanen, M., Rörup, B., Scholz, W., Shen, J., Simon, M., Sipilä, M., Steiner, G., Stolzenburg, D., Tham, Y. J., Tomé, A., Wagner, A. C., Wang, D. S., Wang, Y., Weber, S. K., Winkler, P. M., Wlasits, P. J., Wu, Y., Xiao, M., Ye, Q., Zauner-Wieczorek, M., Zhou, X., Volkamer, R., Riipinen, I., Dommen, J., Curtius, J., Baltensperger, U., Kulmala, M., Worsnop, D. R., Kirkby, J., Seinfeld, J. H., El-Haddad, I., Flagan, R. C., and Donahue, N. M.: Rapid growth of new atmospheric particles by nitric acid and ammonia condensation, Nature, 581, 184–189, https://doi.org/10.1038/s41586-020-2270-4, 2020.

Yiou, P., Salameh, T., Drobinski, P., Menut, L., Vautard, R., and Vrac, M.: Ensemble reconstruction of the atmospheric column from surface pressure using analogues, Clim Dyn, 41, 1333–1344, https://doi.org/10.1007/s00382-012-1626-3, 2013.

Zhang, Y., Favez, O., Petit, J.-E., Canonaco, F., Truong, F., Bonnaire, N., Crenn, V., Amodeo, T., Prévôt, A. S. H., Sciare, J., Gros, V., and Albinet, A.: Six-year source apportionment of submicron organic aerosols from near-continuous highly time-resolved measurements at SIRTA (Paris area, France), 22, 2019.

Zorita, E. and Storch, H. V.: The Analog Method as a Simple Statistical Downscaling Technique: Comparison with More Complicated Methods, 12, 16, 1999.

Zotter, P., Herich, H., Gysel, M., El-Haddad, I., Zhang, Y., Močnik, G., Hüglin, C., Baltensperger, U., Szidat, S., and Prévôt, A. S. H.: Evaluation of the absorption Ångström exponents for traffic and wood burning in the Aethalometer based source apportionment using radiocarbon measurements of ambient aerosol, 1–29, https://doi.org/10.5194/acp-2016-621, 2016.